Operational Ionospheric Correction for SAOCOM Interferometry

Naomi Petrushevsky[a,b], Francesco Banda[b], Andrea Monti-Guarnieri[a], Marc Thibeault[c], Juan Pablo Cuesta Gonzalez[c], and Davide Giudici[b]
[a]Politecnico di Milano, Department of Electronics, Information and Bioengineering, Via Ponzio 34/5, 20133 Milan, Italy
[b]Aresys, Via Privata Flumendosa, 16, 20132 Milano MI, Italy
[c]CONAE, Av. Paseo Colón 751, C1063ACH CABA, Argentina

Abstract

Synthetic Aperture Radar (SAR) systems are widely used for mapping natural scenarios and continuous terrain deformation monitoring. To facilitate correct mapping, any operational processor should effectively estimate and compensate for spurious effects in the acquisitions. A major source of error, especially for systems operating at lower frequencies, is the ionosphere, which biases the phase of the recorded signal. In this paper, we study the application of an ionosphere correction for the SAOCOM L-band system. In particular, we propose an alternative implementation of the split-spectrum algorithm, ready to ingest already coregistered acquisitions. The entire processing chain was tested on a real stack of SAOCOM acquisitions and cross-validated with Faraday-rotation results.

1 Introduction

Synthetic Aperture Radar (SAR) is a remote sensing technique used for numerous operational and experimental platforms to map topography, continuously monitor terrain deformation, retrieve information about natural scenarios, and even 3D mapping. On top of the measured amplitude, the phase of the recorded signal adds another dimensionality to the data space in support of the aforementioned tasks. In particular, SAR interferometry (InSAR) is operationally used to perform fine-scale observations.

To correctly use the acquired data, a preliminary calibration step must be performed to remove disturbances [1]. InSAR techniques are especially sensitive to inaccuracies, making coregistration and phase compensation critical steps in the processing chain. The main sources of errors originate from the estimated orbital positioning, tropospheric delay, and the ionosphere [2]. The latter effect is particularly relevant for low-frequency systems (L-band, P-band).

Variations in the ionosphere's Total Electron Content (TEC) cause several distortions in a SAR image. First, an additional delay is added to the propagation time, and an undesired phase will appear in the InSAR measurements. Furthermore, the ionosphere generates a rotation in the polarimetric channels, known as the Faraday Rotation [3]. Lastly, defocusing may occur due to distortion of the transmitted pulse and variations of electron concentration along the synthetic aperture.

Among the L-band platforms available today, SAOCOM is a constellation of two SAR satellites launched by Argentina's Space Agency (CONAE) in 2018 and 2020 [4]. Each sensor can operate in Stripmap and Terrain Observation with Progressive Scans (TOPS) modes and in different polarimetric configurations: single, dual, and quad-pol. Being an L-band system, SAOCOM acquisitions may be strongly affected by the ionosphere, and processing must account for it to deliver calibrated acquisitions to users.

This paper studies an operational ionospheric correction tool for SAOCOM. In particular, we propose an alternative implementation of the interferometric split-spectrum approach [2], designed to be integrated into a standard InSAR processing chain. The processing takes as input already coregistered acquisitions and performs split-spectrum by introducing a proper phase compensation. The proposed approach is cross-validated with ionosphere phase screens estimated by the Faraday Rotation method, applying both to real SAOCOM acquisitions.

2 Ionospheric Phase Screen

The ionosphere is the atmosphere's upper layer, with a high concentration of free electrons caused by solar radiation. When an electromagnetic (EM) signal travels through the ionosphere, it experiences delays, defocusing, and Faraday Rotation due to circular birefringence [2, 5]. In focused SAR acquisitions, range and azimuth defocusing can be neglected or mitigated [6] and are not handled in this work.

The ionospheric signal (range) delay can be expressed as [7]:

$$\tau_i(f_0+f) = \frac{2K}{c(f_0+f)^2} TEC \tag{1}$$

where $K = 40.28(m^3/s^2)$, TEC is the total electron content experienced by the signal through its propagation (to be here intended as slant TEC), f_0 is the central frequency, and f is the base-band frequency. The total delay of the signal is:

$$\tau(f_0+f) = \tau_{topo} + \tau_{nd} + \tau_i(f_0+f) \tag{2}$$

where τ_{topo} is the part of the propagation time that can be computed from the Digital Elevation Model (DEM), and

ISBN 978-3-8007-6286-6 / ISSN 2197-4403

τ_{nd} is the summation of all other non-dispersive effects such as troposphere and position errors.
When considering an interferometric pair of images, the difference in delays between master and slave $\Delta\tau = \tau_s - \tau_m$ can be estimated and compensated by resampling the slave [8]. Indeed, precise coregistration is crucial for obtaining high coherence.
While misregistration can be solved, dedicated InSAR processing is required to separate ionospheric from non-dispersive components in the signal's phase. The interferometric phase difference can be expressed as:

$$\begin{aligned}&\Delta\phi(f_0+f) = \\ &\quad -\left(2\pi(f_0+f)\Delta\tau_{nd} - 2\pi(f_0+f)\Delta\tau_i(f_0+f)\right)\end{aligned} \tag{3}$$

where f_0 is the central frequency of the common band between master and slave, and the difference in the signs of the last components is due to the dispersive nature of the ionosphere. The expression in (3) considers that the known topographic delay $\Delta\tau_{topo}$ was compensated during preprocessing.

3 Split Spectrum

From Equations (1) and (3), it can be deduced that the signs of the group delay and the phase delay are opposites in the case of the ionosphere. Thus, the ionospheric phase screen can be distinguished and measured by obtaining two sub-bands, each centered around a different frequency. The dispersive phase can then be computed by [9]:

$$\Delta\hat{\phi}_{iono} = \frac{f_L f_H}{f_0(f_H^2 - f_L^2)}\left(f_H\Delta\hat{\phi}_L - f_L\Delta\hat{\phi}_H\right) \tag{4}$$

being $\Delta\hat{\phi}_L$, $\Delta\hat{\phi}_H$ the interferometric phases (3) of the two sub-bands centered around $f_L = f_0 + f_l$ and $f_H = f_0 + f_h$, respectively. Considering the demodulated signal, f_l and f_h are the frequencies of the low and high sub-bands.
Note that the split-spectrum method cannot be applied to a single image since, in the general case, the phase of the target randomly changes between the bands. Thus, an InSAR approach is utilized, eliminating the phase contributions related to the specific target:

$$\Delta\hat{\phi}_{L/H} = \angle\mathbb{E}\left[s_{L/H}\cdot m^*_{L/H}\right] \tag{5}$$

where $m_{L/H}$ and $s_{L/H}$ are the master and slave signals for the relevant band, and the expected value is computed by averaging over a moving window.

3.1 Compensating the Effect of Coregistration

The spectra of the demodulated and focused master (M) and slave (S) signals, are:

$$\begin{aligned}M(f) =& A(f)\\ S(f) =& A(f)e^{-j2\pi f_0(\Delta\tau_{topo}+\Delta\tau_{nd}-\Delta\tau_i(f_0))}\\ &\cdot e^{-j2\pi f(\Delta\tau_{topo}+\Delta\tau_{nd}+\Delta\tau_i(f_0+f))}\end{aligned} \tag{6}$$

where $A(f)$ is the observed spectrum of the scene after demodulation. The slave has two additional exponentials: the first is the interferometric phase, while the second defines the shift between the images. Without loss of generality, since we are looking at differential contributions, all the phase terms were assigned to the slave data.
State-of-the-art works about the split spectrum algorithm generate the two sub-bands from the focused data [2, 10]. Next, each band is demodulated and resampled separately, and the topographic phase is removed. Note that the resampling does not change the measured phase. Following such a scheme, the slave's sub-band centered around f_L can be expressed as:

$$\begin{aligned}S_{L,c}(f) &= A_L(f)e^{j\Delta\phi(f_L)}\\ A_L(f) &= A(f)\cdot\mathrm{rect}\left(\frac{f-f_l}{B}\right)\end{aligned} \tag{7}$$

where the same holds for the band centered around f_H, and the explicit definition of $\Delta\phi$ is given in (3). B is the sub-band width, and the notation $[.]_{L,c}$ indicates that filtering was performed before coregistration. Finally, the interferometric phases between master and slave bands $\Delta\phi(f_L)$ and $\Delta\phi(f_H)$ can be directly used for the estimation of the ionospheric phase screen (4).
In our case, the dispersive phase estimation must comply with a standard preprocessing chain, highlighted in blue in Fig.1. Thus, sub-bands must be obtained from images that are already coregistered and phase-compensated. In this section, we derive the interferometric phase of the bands generated after coregistration and suggest a method to adjust them for the correct split spectrum implementation.
The resampling shifts $\hat{\tau}$ are obtained directly from the data by performing incoherent speckle tracking [11] between master and slave. The estimated shifts are measured after common-band filtering, so both spectra are centered around f_0:

$$\hat{\Delta}\tau_{coreg}(f_0) = \Delta\tau(f_0) + \Delta\tau_{err} \tag{8}$$

Where $\Delta\tau_{err}$ is the coregistration error. The shifts in (8) are applied to the slave, and the known topographic phase $2\pi f_0\tau_{topo}$ is removed. The described steps conclude a standard InSAR processing procedure. At this point, two bands are extracted and demodulated, so the phase of each band can be obtained by combining (2), (3) and (8):

$$\begin{aligned}&S_{c,L}(f) = \\ &A_L(f)e^{j\Delta\phi(f_0)}e^{j2\pi f(\Delta\tau_i(f_0)-\Delta\tau_i(f_L))+j2\pi f\Delta\tau_{err}}\end{aligned} \tag{9}$$

Observing (7) and (9), it is clear that the band obtained after coregistration cannot be directly used for the ionosphere estimation. However, the bias can be resolved by applying to each look the following phase term:

$$\begin{aligned}\phi_d(f) &= -2\pi f(\Delta\hat{\tau}_{coreg} - \Delta\tau_{topo})\\ &= -2\pi f(\Delta\tau_{nd} + \Delta\tau_i(f_0) + \Delta\tau_{err})\end{aligned} \tag{10}$$

The correction phase can be computed directly from the estimated shifts and the known topographic pattern. The

ISBN 978-3-8007-6286-6 / ISSN 2197-4403

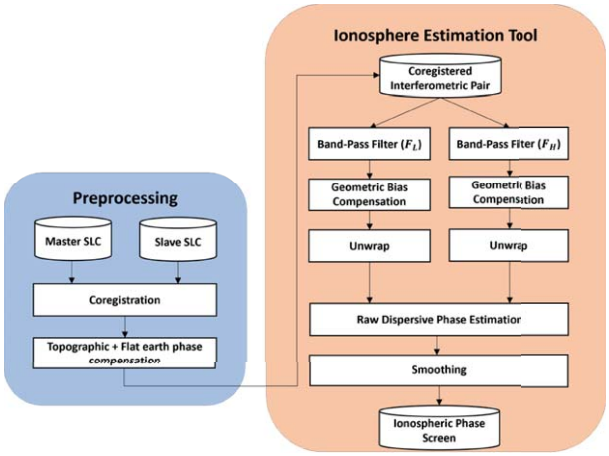

Figure 1 Proposed ionospheric phase screen estimation.

compensated band will be:

$$\begin{aligned} & S_{c,L}(f) \cdot e^{j\phi_d(f_L)} \\ & \quad = A_L(f) e^{j\Delta\phi(f_0)} e^{-j2\pi f(\Delta\tau_{nd} - \Delta\tau_i(f_L))} \\ & \quad \approx A_L(f) e^{\Delta\phi(f_L)} \end{aligned} \tag{11}$$

Thus, we can generate the sub-bands after coregistration and apply the phase correction introduced in (10). The result is equivalent to the alternative approach, known from the literature, where bands are generated prior to coregistration (see (7)).

3.2 Operational processing

The complete block scheme of the proposed ionosphere phase screen estimation tool is reported in Fig.1. The preprocessing part (marked in blue) is a standard routine that outputs coregistered acquisitions, including nominal geometry compensation from an external DEM. The core of the ionospheric processing (marked in orange) is the split spectrum algorithm modified to account for already resampled acquisitions as explained in Section 3.1. The steps are described in the following.

After generating two sub-bands, each occupying one-third of the entire spectrum [2], interferograms between the master and the slave are computed. The phase bias caused by the coregistration is then removed from each interferogram, according to (10). Both data are unwrapped and used as input for the split spectrum equation (4). The result at this stage is noisy, and additional smoothing is performed by bivariate splines, using coherence values as weights. Validation of the proposed implementation is provided in Section. 5.

4 Faraday Rotation

As discussed in Section 1, the ionosphere rotates the polarization plane of a SAR signal. Faraday Rotation can be measured and converted into an ionospheric phase screen from single acquisitions when quad-polarization is available. We use this approach as a cross-validation for our split-spectrum implementation.

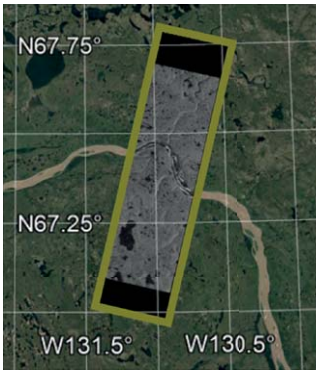

Figure 2 An example of a geocoded acquisition intensity image of the data. The scene is located in north Canada.

Given four polarimetric channels $[Y_{vv}, Y_{vh}, Y_{hv}, Y_{hh}]$, the Faraday rotation angle can be measured by [12]:

$$\begin{aligned} \Omega &= \frac{1}{4} \angle \left[Y_{2,1} Y_{1,2}^* \right] \\ Y_{1,2} &= \frac{Y_{hh} - iY_{hv} + iY_{vh} + Y_{vv}}{2} \\ Y_{2,1} &= \frac{Y_{hh} + iY_{hv} - iY_{vh} + Y_{vv}}{2} \end{aligned} \tag{12}$$

where $*$ stands for the complex conjugate.

To convert the rotation angle expressed in (12) into a dispersive phase screen, one can utilize the following relation:

$$\phi_{iono}^{farad} = \frac{4\pi f_0 \cdot m}{e \cdot B_{||}} \Omega \tag{13}$$

being m and e the mass and the charge of an electron, respectively. $B_{||}$ is the component of the magnetic field in the direction of the line of sight (LOS).

Faraday rotation is an absolute measure, i.e., it requires only one image. To compare the results to the split-spectrum based solution, the differential between a master and a slave is computed:

$$\Delta\phi_{iono}^{farad} = \phi_{iono,S}^{farad} - \phi_{iono,M}^{farad} \tag{14}$$

While the conversion of Faraday rotation to phase is straightforward, it requires some care, as accurate information about ionospheric height and magnetic field are needed. First, the magnetic field was retrieved from the International Geomagnetic Reference Field (IGRF) model [13] and was interpolated at the corresponding piercing point (see Fig.3). The ionosphere is usually modeled as a thin layer at a given height. The precise height changes over time and position and was retrieved from the International Reference Ionosphere [14].

5 Experimental Results

Validation of the proposed split-spectrum implementation (Fig.1) is done with real SAOCOM-1A acquisitions collected over North Canada (Fig.2). The used polarimetric channel is HH and the resolution of the data is 6m in azimuth and 6m in slant-range. It has to be remarked that focusing our analysis at higher latitudes is important to allow

ISBN 978-3-8007-6286-6 / ISSN 2197-4403

Figure 3 Geometry of ionosphere estimation: the acquired scene in yellow, ionosphere piercing area in orange, and the position of the satellite during acquisition is in red.

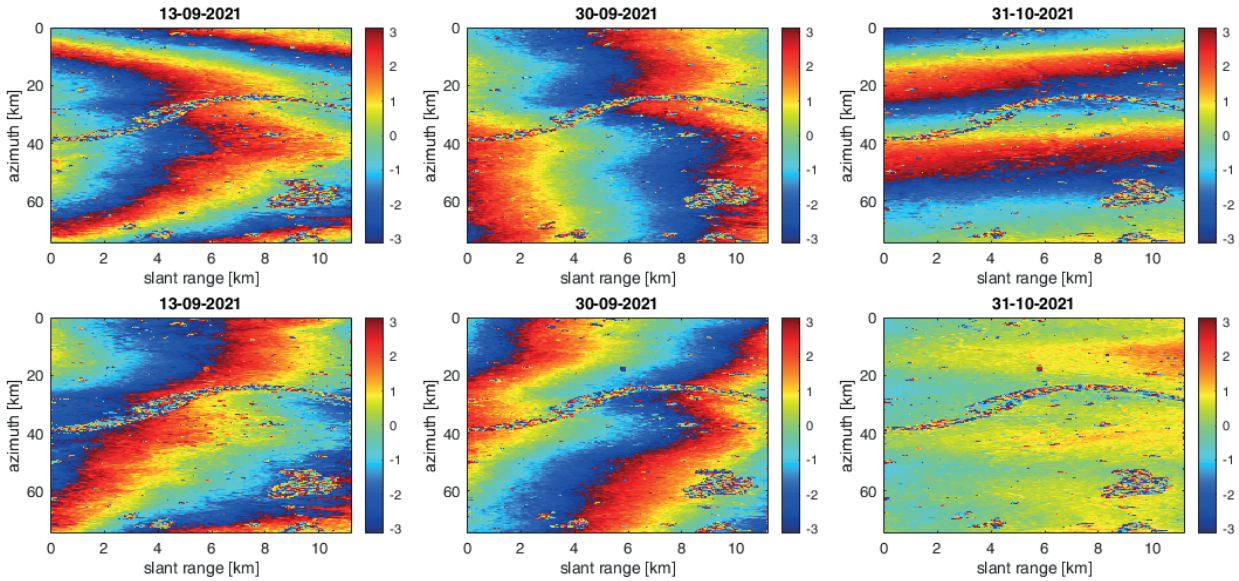

Figure 4 SAOCOM interferograms: original phases (top) and compensated phases after removal of ionospheric phase screen (bottom). The interferograms were computed with a local window of 25m $\times$ 22m in range and azimuth, respectively.

Table 1 SAOCOM acquisition used for testing the operational tool for ionospheric phase screen estimation.

	Date	Normal baseline
1	13/09/2021	403m
2	30/09/2021	72m
4	14/10/2021	0m
4	31/10/2021	611m

comparison with the Faraday rotation correction method since the latter has reduced sensitivity close to the magnetic Equator [12]. The geometry of the acquisition is shown in Fig.3. The ionospheric piercing area was computed from the satellite orbits and the ionosphere's height during the relevant period, which was 240km.

The dates and normal baselines of the four acquisitions used in the present analysis are reported in table 1, where the master acquisition is identified as the one with a zero baseline. The three original interferograms generated with respect to the common master are shown in Fig.4, with a local averaging window of 25 $m \times 22$ m in slant-range and azimuth. Clear phase trends are visible; however, it is not possible to determine apriori if the patterns are due to ionosphere or other non-dispersive effects such as troposphere or positioning errors.

The estimation of the ionospheric phase screen was performed as described in Fig.1. Due to the strong noise amplification consequent to the split-spectrum method [2] and the slow varying nature of the ionosphere, a large window was used for estimating the phase of each sub-band, i.e., 100m $\times$ 88m in slant range and azimuth, respectively. The raw dispersive phase, resulting from (4), is shown in the top part of Fig.5. A clear phase gradient is visible in all three images, mainly along azimuth. However, the phase is still very noisy and cannot be applied as is to the original interferograms. The bottom part of Fig.5 shows the resulting phase screens after smoothing with bivariate splines.

The compensated phases are provided in the bottom of Fig.4. It is clear that some other non-dispersive effects are present in the first two interferograms, possibly due to troposphere or coregistration errors. The last phase pattern in the time series is much flatter, with slight variations along range.

ISBN 978-3-8007-6286-6 / ISSN 2197-4403

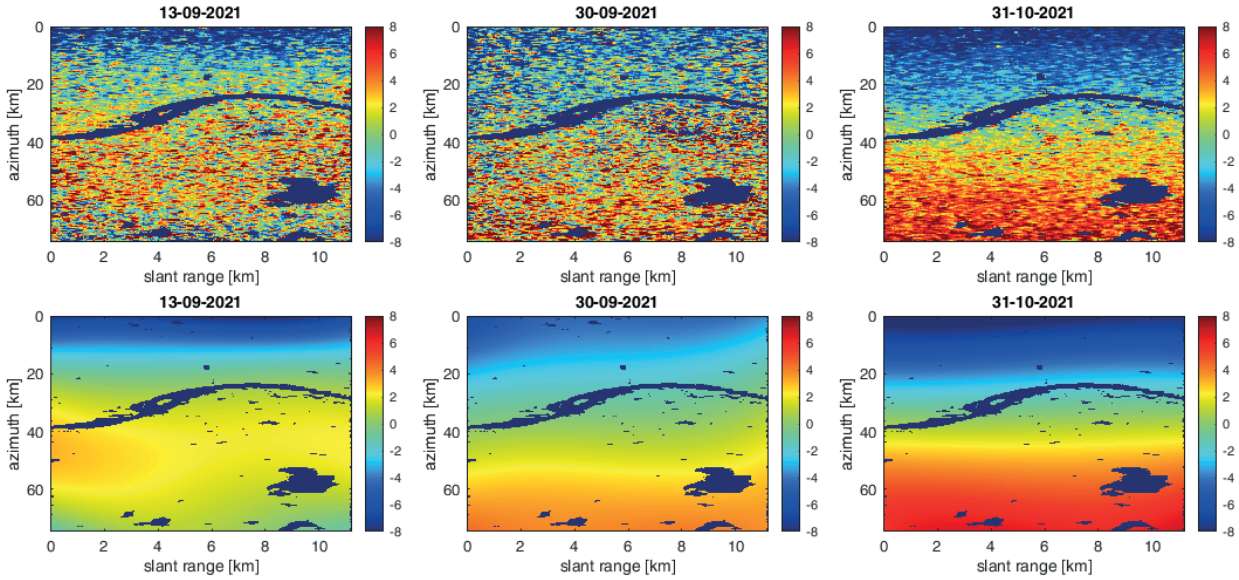

Figure 5 Estimated Ionospheric phase screen by the proposed processing chain. Raw phase screens (top) show a clear variation but are very noisy. The smoothed screens (bottom) can be compensated from the original interferograms.

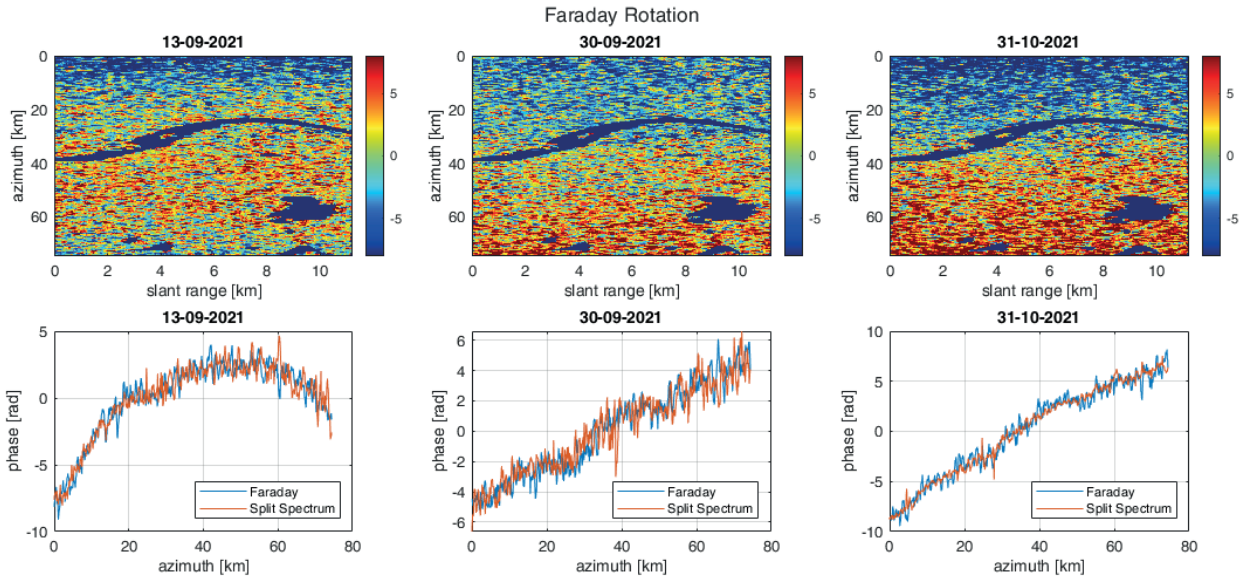

Figure 6 Validation of the proposed split-spectrum approach by the Faraday rotation based method. Top: ionospheric phase screens obtained by converting the measured Faraday rotation to phase. Bottom: azimuth profile of the estimated phase screens for both methods.

To validate the obtained results, we performed a parallel estimation of the dispersive phase screen using the Faraday rotation method, as described in Section 4. The same averaging window was used as for the split-spectrum approach. The corresponding ionospheric phase is shown in Fig.6. Top panels report estimated phase screens, where trends similar to those computed by split-spectrum processing appear. For a better comparison between the two approaches, azimuth profiles were extracted by averaging along the range direction. As shown in the bottom panels of Fig.6, a strong agreement between profiles is obtained in all three cases, validating the proposed technique.

6 Conclusions

In this work, we propose an alternative implementation of the split-spectrum algorithm targeted for an operational SAOCOM InSAR processor. The solution is adapted to take as input already coregistered data by introducing a proper phase compensation. This way, the entire chain can be executed after standard InSAR pre-processing procedures.

Cross-validation of the proposed ionospheric phase screen estimation and compensation is done by comparing the results with a Faraday rotation estimation. The comparison was possible due to the availability of full-polarimetric

ISBN 978-3-8007-6286-6 / ISSN 2197-4403

SAOCOM data by converting the estimated rotation angle into an ionospheric phase screen. The results obtained with this method agree well with the phase screens estimated by the split-spectrum proposed scheme.

Split-spectrum and Faraday rotation are both well-validated methods for measuring the TEC experienced during SAR acquisitions. Although Faraday rotation is able to provide information from one image, it was not the focus of this study because its sensitivity highly depends on the direction of the magnetic field; indeed, it cannot be applied in equatorial regions. Moreover, the conversion of the Faraday rotation into phase requires precise knowledge about the true conditions of the magnetic field and ionospheric 3-D structure, both of which were retrieved from external sources. Hence, a split-spectrum based approach was considered here, and Faraday rotation was used as a cross-validation tool.

Further analysis should be carried out to examine the bias introduced by large interferometric baselines, as described in [2]. Moreover, the evaluation of additional test sites is programmed, gaining from the ability of the method to operate on existing interferometric stacks without any reprocessing.

7 Literature

[1] A. Ferretti, C. Prati, and F. Rocca. Permanent scatterers in SAR interferometry. *IEEE Transactions on Geoscience and Remote Sensing*, 39(1):8–20, January 2001. Conference Name: IEEE Transactions on Geoscience and Remote Sensing.

[2] Giorgio Gomba, Alessandro Parizzi, Francesco De Zan, Michael Eineder, and Richard Bamler. Toward Operational Compensation of Ionospheric Effects in SAR Interferograms: The Split-Spectrum Method. *IEEE Transactions on Geoscience and Remote Sensing*, 54(3):1446–1461, March 2016.

[3] P.A. Wright, S. Quegan, N.S. Wheadon, and C.D. Hall. Faraday rotation effects on L-band spaceborne SAR data. *IEEE Transactions on Geoscience and Remote Sensing*, 41(12):2735–2744, December 2003. Conference Name: IEEE Transactions on Geoscience and Remote Sensing.

[4] Laura Fioretti, Davide Giudici, Pietro Guccione, Andrea Recchia, and Martin Steinisch. SAOCOM-1B Independent Commissioning Phase Results. In *2021 IEEE International Geoscience and Remote Sensing Symposium IGARSS*, pages 1757–1760, July 2021. ISSN: 2153-7003.

[5] Michael Jehle, Maurice Ruegg, Lukas Zuberbuhler, David Small, and Erich Meier. Measurement of Ionospheric Faraday Rotation in Simulated and Real Spaceborne SAR Data. *IEEE Transactions on Geoscience and Remote Sensing*, 47(5):1512–1523, May 2009. Conference Name: IEEE Transactions on Geoscience and Remote Sensing.

[6] Francesco Banda, Simone Mancon, Mauro Mariotti D'Alessandro, Stefano Tebaldini, Davide Giudici, Muriel Pinheiro, and Klaus Scipal. BIOMASS INTERFEROMETRIC CALIBRATION PROCESSOR DESIGN. In *IGARSS 2023. 2023 IEEE International Geoscience and Remote Sensing Symposium*.

[7] Franz J Meyer and Jeremy Nicoll. The Impact of the Ionosphere on Interferometric SAR Processing. In *IGARSS 2008 - 2008 IEEE International Geoscience and Remote Sensing Symposium*, volume 2, pages II–391–II–394, July 2008. ISSN: 2153-7003.

[8] Zhengxiao Li and James Bethel. IMAGE COREGISTRATION IN SAR INTERFEROMETRY. 2008.

[9] Paul A. Rosen, Scott Hensley, and Curtis Chen. Measurement and mitigation of the ionosphere in L-band Interferometric SAR data. In *2010 IEEE Radar Conference*, pages 1459–1463, May 2010.

[10] Cunren Liang, Piyush Agram, Mark Simons, and Eric J. Fielding. Ionospheric Correction of InSAR Time Series Analysis of C-band Sentinel-1 TOPS Data. *IEEE Transactions on Geoscience and Remote Sensing*, 57(9):6755–6773, September 2019. Conference Name: IEEE Transactions on Geoscience and Remote Sensing.

[11] Francesco De Zan. Accuracy of Incoherent Speckle Tracking for Circular Gaussian Signals. *IEEE Geoscience and Remote Sensing Letters*, 11(1):264–267, January 2014. Conference Name: IEEE Geoscience and Remote Sensing Letters.

[12] Jun Su Kim, Konstantinos P. Papathanassiou, Rolf Scheiber, and Shaun Quegan. Correcting Distortion of Polarimetric SAR Data Induced by Ionospheric Scintillation. *IEEE Transactions on Geoscience and Remote Sensing*, 53(12):6319–6335, December 2015.

[13] P. Alken, E. Thébault, C. D. Beggan, et al. International Geomagnetic Reference Field: the thirteenth generation. *Earth, Planets and Space*, 73(1):49, February 2021.

[14] Dieter Bilitza. IRI the International Standard for the Ionosphere. In *Advances in Radio Science*, volume 16, pages 1–11. Copernicus GmbH, September 2018. ISSN: 1684-9965.

ISBN 978-3-8007-6286-6 / ISSN 2197-4403